What We Can Learn from the Norms of One-Particle Density Matrices, and What We Can't: Some Results for Interstate Properties in Model Singlet Fission Systems

ARTICLE *in* THE JOURNAL OF PHYSICAL CHEMISTRY A · JULY 2014

Impact Factor: 2.69 · DOI: 10.1021/jp506090g · Source: PubMed

4 AUTHORS, INCLUDING:

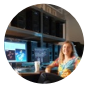

Anna I Krylov
University of Southern California
179 PUBLICATIONS **7,028** CITATIONS

SEE PROFILE

THE JOURNAL OF PHYSICAL CHEMISTRY A

Article

pubs.acs.org/JPCA

What We Can Learn from the Norms of One-Particle Density Matrices, and What We Can't: Some Results for Interstate Properties in Model Singlet Fission Systems

Spiridoula Matsika,[†] Xintian Feng,[‡] Anatoliy V. Luzanov,[§] and Anna I. Krylov*[,‡]

[†]Department of Chemistry, Temple University, Philadelphia, Pennsylvania 19122, United States

[‡]Department of Chemistry, University of Southern California, Los Angeles, California 90089-0482, United States

[§]STC "Institute for Single Crystals", National Academy of Sciences, Kharkov 61001, Ukraine

Supporting Information

ABSTRACT: The utility of the norms of one-particle density matrices, $\|\gamma\|$, for understanding the trends in electronic properties is discussed. Using several model systems that are relevant in the context of singlet fission (butadiene, octatetraene, and ethylene dimer), the dependence of interstate properties (such as transition dipole moments and nonadiabatic couplings, NACs) on molecular geometries is investigated. $\|\gamma\|$ contains the principal information about the changes in electronic states involved, such as varying degree of one-electron character of the transition; thus, it captures leading trends in one-electron interstate properties (i.e., when $\|\gamma\|$ is small, the respective interstate matrix elements are also small). However, finer variations in properties that arise due to the dependence of the matrix elements of the respective operators may not be reproduced. Analysis of NACs in ethylene dimer reveals that intermolecular components of NACs follow the trends in $\|\gamma\|$ well, as they are determined primarily by the characters of the two wave functions; however, intramolecular components depend on the relative orientation of the two moieties via the dependence in the derivative of the electron−nuclear Coulomb operator. Therefore, intramolecular NACs may exhibit large variations even when the changes in $\|\gamma\|$ are small. We observe large NACs at perfectly stacked geometry; however, larger values (by a factor of 1.6) are observed at slip-stacked (along the long axis) geometries. Larger values of NACs at slip-stacked configurations are due to the breaking of symmetry of the local environment of the heavy atoms and not due to the wave function composition. We found that the variations in $\|\gamma\|$ for ethylene dimer are due to a varying admixture of the charge-resonance configurations in the S_1 state, whereas the ^{1}ME state retains its pure multiexciton character.

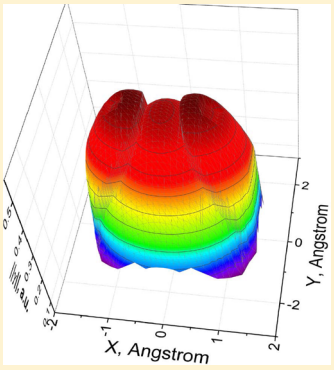

1. INTRODUCTION

Reduced density matrices (DMs)[1−4] are widely used in many-body theories, both for quantitative and qualitative purposes. They allow one to compress the information contained in many-electron wave functions such that only essential details are preserved. The utility of DMs stems from the basic quantum-mechanical result due to the indistinguishability of the electrons. One can easily show that in order to compute an expectation value of a one-particle operator, $\hat{A} = \sum_{pq} A_{pq} p^+ q$, only a one-particle DM (OPDM), γ, is needed:

$$\langle \Psi | \hat{A} | \Psi \rangle = \mathrm{Tr}[A\gamma] = \sum_{pq} A_{pq}\gamma_{qp} \tag{1}$$

where

$$\gamma_{qp} \equiv \langle \Psi | p^+ q | \Psi \rangle \tag{2}$$

Here and below we employ second quantization formalism; p^+ and q denote creation and annihilation operators, respectively, and the sums run over all basis functions. Any orthonormal spin−orbital basis can be used; eq 1 is orbital-invariant.[5] Likewise, two-particle DMs can be used to compute expectation values of two-electron operators, and so forth.

In a similar fashion, the so-called transition DMs can be defined and used to compute interstate properties such as couplings and transition dipole moments:

$$\langle \Psi_i | \hat{A} | \Psi_f \rangle = \mathrm{Tr}[A\gamma^{if}] \tag{3}$$

$$\gamma^{if}_{qp} \equiv \langle \Psi_i | p^+ q | \Psi_f \rangle \tag{4}$$

where i and f denote the initial and final states, respectively. Since the focus of this work is on interstate properties and transition DMs, the superscript if will be dropped in the presentation that follows.

Equations 1 and 3 are routinely used in electronic structure codes to compute one-electron properties. By virtue of these equations, the code for properties calculations is the same for

Special Issue: David R. Yarkony Festschrift

Received: June 18, 2014
Revised: July 27, 2014
Published: July 28, 2014

various approximate wave functions. Once wave function amplitudes are obtained, one can compute the required DMs and discard the amplitudes thus avoiding storage bottlenecks in the subsequent calculations.

We note that for properties associated with real-valued Hermitian operators and real-valued wave functions only the symmetric part of OPDM, γ^s, contributes to the computed matrix elements:

$$\gamma^s_{pq} \equiv \frac{1}{2}(\gamma_{pq} + \gamma_{qp}) \tag{5}$$

OPDMs are also very useful for the interpretation and qualitative wave function analysis. OPDM defined by eq 2 gives the expansion coefficients for representing electron density ρ in the basis of molecular (or atomic) orbitals:

$$\rho(r) = \sum_{pq} \gamma_{pq}\phi_p(r)\,\phi_q(r) \tag{6}$$

Thus, the trace of γ equals the number of the electrons. Consequently, OPDMs can be used to define and compute quantities such as atomic charges, bond orders, and so forth, which are exploited in Mulliken and Löwdin population analyses,[6] as well as in more sophisticated Atom-in-Molecule, Natural Bond Orbital, and Natural Resonance theories.[7−9]

OPDMs also contain information about the correlation, which can be used for the analysis of the electronic structure. For example, Yamaguchi and Head-Gordon indexes[10,11] and the related particle−hole occupancies[12] allow one to quantify the effective number of unpaired electrons.

In the context of excited states, OPDMs can be used to describe the character of the electronic transitions in terms of the orbitals involved, as done in the attachment−detachment analysis, natural transition orbitals, and other approaches.[13−16] These orbital-invariant schemes allow one to focus on the essential features of wave functions; they become critically important when the wave function includes multiple amplitudes with similar weights (see, for example, ref 17). Furthermore, one can use OPDMs for assigning the character of the transitions as charge-transfer or local excitations.[15,16,18−20] Transition OPDMs can be used for visualizing excitons, computing average particle−hole distances, and more.[12,20]

The focus of this work is on a quantity that has not received much attention yet, the norm of OPDM:

$$\|\gamma\| \equiv \sqrt{\sum_{pq} (\gamma_{pq})^2} = \sqrt{\mathrm{Tr}[\gamma\gamma^+]} \tag{7}$$

where the orthonormal basis is implied. Note that

$$\|\gamma\|^2 = \|\gamma^s\|^2 + \|\gamma^{as}\|^2 \tag{8}$$

where $\gamma^{as}_{pq} \equiv 0.5(\gamma_{pq} - \gamma_{qp})$. Thus, the norm of symmetrized γ is always smaller than $\|\gamma\|$. For pure one-electron excitations:

$$\|\gamma^s\| = \|\gamma^{as}\| = \frac{\|\gamma\|}{\sqrt{2}} = \frac{1}{\sqrt{2}} \tag{9}$$

$\|\gamma\|$ was recently used to analyze trends in nonadiabatic couplings (NACs) in the context of singlet fission[21−23] and to explain the behavior of resonance wave functions in calculations using complex absorbing potentials (CAPs).[24] In this work we provide more detailed description of the formalism and illustrate its utility by several examples, with an emphasis on interstate properties such as transition dipole moments (μ_{tr}) and NACs.

NAC matrix elements are the central quantities in nonadiabatic processes:

$$\langle \Phi_i(r; R)|\nabla_R \Phi_f(r; R)\rangle \tag{10}$$

where $\Phi_i(r;R)$ and $\Phi_f(r;R)$ are electronic wave functions of the initial and final states. We note that this coupling is a vector in the space of nuclear displacements; in rates' calculations, it should be contracted with a respective component of the nuclear momentum, $\nabla_R\xi$ (ξ denotes nuclear wave function). The structure of this vector and its relation to the topology of conical intersections has been analyzed in detail by David Yarkony.[25−27]

Equation 10 is never used for practical calculations;[28−33] instead one can easily show that[34]

$$\langle \Phi_i(r; R)|\nabla_R \Phi_f(r; R)\rangle = \frac{\langle \Phi_i|\nabla_R \hat{H}_{el}|\Phi_f\rangle}{U_f - U_i} \tag{11}$$

where U_i and U_f are electronic energies of the initial and final states. This can be derived from the Schroedinger equation by either simple differentiation or by using perturbation theory and Taylor expansion around a fixed nuclear geometry. In derivation of eq 11, we employ Hellman−Feynman theorem; thus, for approximate solutions of electronic Schroedinger equations additional terms containing $\nabla_R\Phi$ may appear; these so-called Pulay terms can be tackled by the response theory (or by the Lagrangian technique), as done in analytic nuclear gradient formalism.[35] Such theoretically complete formalism and its computer implementation for MR-CI wave functions have been first developed by David Yarkony and co-workers.[28−30,36,37] More recently, this formalism has been applied to the CIS and TDDFT methods;[31−33] analytic derivative matrix elements have also been computed for equation-of-motion coupled-cluster wave functions in order to parametrize vibronic Hamiltonian.[38]

The only part of the electronic Hamiltonian that explicitly depends on nuclear coordinates is $\hat{V}_{en}$:

$$\frac{\partial \hat{H}_{el}}{\partial R} = \frac{\partial \hat{V}_{en}}{\partial R} = -\frac{\partial}{\partial R}\left(\sum_{A,i} \frac{Z_A}{|r_i - R_A|}\right) \tag{12}$$

where the sum runs over all atoms and all electrons.

Although $\hat{V}_{nn}$ also depends on nuclear coordinates, the respective contributions to NAC vanish because of the orthonormality of the electronic wave functions. Thus, in the case of the exact wave functions, NAC is a strictly one-electron operator and can be computed using unrelaxed OPDM given by eq 4:

$$\langle \Phi_i(r; R)|\nabla_R \Phi_f(r; R)\rangle = \frac{\mathrm{Tr}[\gamma^{if} V^R]}{U_f - U_i} \tag{13}$$

where V^R is the matrix of the operator $\hat{V}^R_{en} \equiv \partial\hat{V}_{en}/\partial R$. Note that NAC is anti-Hermitian, $\langle \Phi_i|\nabla\Phi_j\rangle = -\langle \Phi_j|\nabla\Phi_i\rangle$, owing to the energy difference denominator, whereas the derivative operator, $\hat{V}^R$, is Hermitian (thus, a symmetrized γ^{if} can be used for its evaluation).

When approximate solutions are used, eq 13 needs to be modified. First, non-Hellman−Feynman terms should be accounted for by solving amplitude and orbital response equations. Their effect can be trivially folded into the DMs leading to the so-called relaxed DMs:

dx.doi.org/10.1021/jp506090g | J. Phys. Chem. A 2014, 118, 11943−11955

$$\langle \Phi_i(r; R)|\nabla_R \Phi_f(r; R)\rangle = \frac{1}{U_f - U_i}(\mathrm{Tr}[h^R\tilde{\gamma}] + \mathrm{Tr}[II^R\tilde{\Gamma}]) \quad (14)$$

where h^R and II^R denote the derivatives of the one- and two-particle parts of H_{el}; $\tilde{\gamma}$ and $\tilde{\Gamma}$ are the relaxed one- and two-particle transition DMs, respectively. Note that when incomplete atom-centered one-electron basis sets are used, the full expression of NAC contains contributions from other parts of H_{el} (such as kinetic energy and electron repulsion integrals) due to the implicit dependence of the matrix elements on the one-electron basis. Thus, the two-electron contributions to NAC are artifacts of using atom-centered incomplete basis sets; they vanish in the complete basis set limit or when using non-AO bases, such as plane-wave or grid representations. Interestingly, the correction restoring translational invariance of NACs exactly cancels out the non-Hellman−Feynman contribution to NACs in the CIS and TDDFT models.[33]

The differences between the relaxed and unrelaxed DMs are usually small. While they are indispensable for calculating the nuclear gradient, their effect on the computed properties is insignificant and is often ignored. In particular, orbital response terms are usually excluded from the properties calculations because they introduce poor pole structure.[35]

Thus, in the limit of complete basis set, γ_{pq} is all that is needed to compute NAC, which is described by one-electron operator $\hat{V}^R_{en}$:

$$\langle \Phi_i|\hat{V}^R_{en}|\Phi_f\rangle = \mathrm{Tr}[\gamma^{if}V^R_{en}] \quad (15)$$

In this paper, we investigate NACs computed by full analytic formulation for several model systems relevant to singlet fission;[39−41] we compare trends in NACs and other properties (i.e., dipole moments) with trends in $\|\gamma\|$. We also investigate the origin of NACs in ethylene dimer.[40]

The structure of the paper is as follows. The next section presents the formalism, followed by the computational details. The numeric examples are presented and discussed in section IV. Additional properties of OPDMs are described in Appendix A. Appendix B outlines calculations of rates of nonadiabatic processes by using the Fermi Golden Rule. Appendix C analyses multiexciton wave functions for a model four-electrons-in-four-orbitals case.

II. THEORY

We begin by applying the Cauchy−Schwartz inequality to eqs 1 and 3:

$$|\mathrm{Tr}[A\gamma]| = |\sum_{pq} A_{pq}\gamma_{qp}| \le \|A\|\cdot\|\gamma\| \quad (16)$$

Thus, $\|\gamma\|$ provides a bound to the respective expectation values (or matrix elements describing interstate properties).

An attractive property of $\|\gamma\|$ is that it is independent of the (orthonormal) orbital basis (i.e., matrix-invariant). For example, it is not affected by the unitary transformations between localized and delocalized molecular orbitals. However, the Frobenius norm of γ is different in the MO and AO bases.[42] Thus, one needs to be consistent when applying eq 16 and to compare the trends using either the MO or AO basis only. The discrepancy can be avoided by computing operator norms correctly in a nonorthonormal basis, i.e., by using

$$\|\gamma\| = \mathrm{Tr}[\gamma S\gamma^+ S] \quad (17)$$

where S is a covariant overlap matrix and γ is a contravariant density matrix in the AO basis. In the MO basis (or an orthogonal AO basis) $S = 1$; thus, this equation reduces to eq 7. In this paper, we always compute γ in the MO basis or in the orthonormal Löwdin AO basis.

Equation 16 is valid both for permanent properties, when γ is given by eq 2, as well as for interstate properties. We first discuss the latter. For interstate properties, γ is given by eq 4; it describes the re-distribution of the electron density associated with the $i \to f$ transition (note that in general the transition density is not equal to the density differences). It was suggested[21] that $\|\gamma\|$ can be considered as a measure of the magnitude of a one-electron interstate property when matrix representation of the respective operator is not available. It was also speculated that in the context of condensed phase where one expects significant modulations in matrix elements due to finite-temperature sampling one can assume random fluctuations in the matrix elements of A; thus, it is reasonable to assume that statistically averaged NAC is proportional to (or, more precisely, symbatic with) $\|\gamma\|$. In the next section, we present numeric investigations of the validity of these assumptions.

To better understand eq 16, we note that

$$|\mathrm{Tr}[\gamma A]| = \|\gamma\|\cdot\|A\|\cdot\cos(\alpha) \quad (18)$$

where α is an angle between the two multidimensional vectors, A and γ, *defined* by the above equation. This form illustrates that if the angle remains constant as a function of certain parameters (e.g., changing nuclear geometries), then one can readily estimate trends in $|\mathrm{Tr}[\gamma A]|$ by considering $\|\gamma\|$ and $\|A\|$. If one of the norms is constant, then the trends in the other provide useful information (but not the other way around). Of course, if two vectors are orthogonal ($\alpha = \pi/2$) or if both quantities significantly change their magnitude, eq 16 is not useful. Another special case is when one quantity changes its orientation and magnitude at random—in this case averaging can be performed giving rise to a constant factor.

In the context of interstate properties, we note that γ_{pq} provides a measure of a one-electron character of the transition between $|\Phi_i\rangle$ and $|\Phi_f\rangle$. Specifically, $\mathrm{Tr}[\gamma\gamma^+]$ can be interpreted as the number of electrons associated with one-electron excitation connecting the two states. For example, this quantity is one for purely one-electron excitation (e.g., for any Hartree−Fock/CIS states) and is zero (no one-electron character) for purely doubly excited states. Thus, when $|\Phi_i\rangle$ and $|\Phi_f\rangle$ differ by two or more excited electrons, matrix elements of any one-electron interstate property should be zero. Some interesting sum rules for the squared norms, $\|\gamma\|^2$, are derived in the Appendix.

We now consider eq 16 in the context of state properties, when γ represents OPDM of a given electronic state. A useful aspect of eq 16 is that it highlights the connection between the density and various observables. For example, in ref 24 this equation was employed to map the trends in the spatial extent of the electronic wave function (as measured by $\langle R^2\rangle$) and its energy in the context of resonances and CAPs. In CAP-augmented electronic structure calculations, the resonances (metastable electronic states embedded in the ionization continuum) are stabilized by the CAP. It was observed that as the strength of CAP increases, the size of the wave function shrinks; once the critical strength is achieved, the wave function

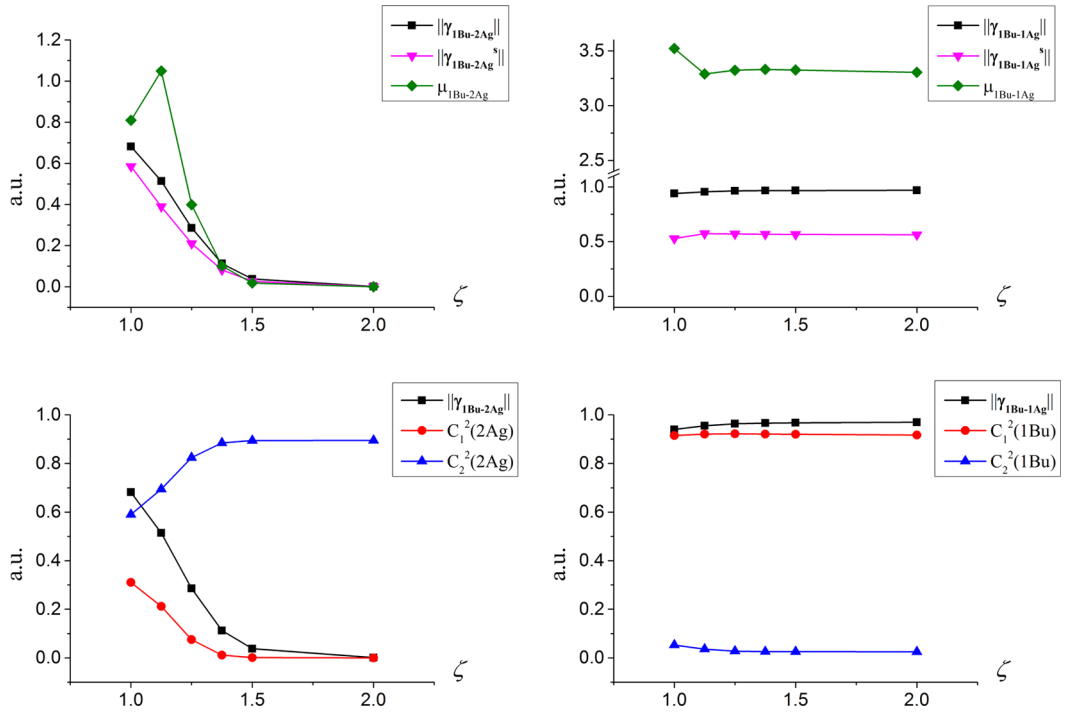

Figure 1. Stretching of octatetraene along C4−C5 (ζ is the bond stretching parameter, $\zeta = 1$ corresponds to the r_e). Top: Matrix elements of the dipole operator (a.u.) and $\|\gamma\|$ between the $2A_g$ and $1B_u$ states (left) and between $1A_g$ and $1B_u$ states (right). γ^s denotes symmetrized OPDM. Bottom left: Weights of singly (C_1^2) and doubly (C_2^2) excited configurations in the $2A_g$ wave function and $\|\gamma_{1B_u-2A_g}\|$. Bottom right: Weights of singly (C_1^2) and doubly (C_2^2) excited configurations in the $1B_u$ wave function and $\|\gamma_{1B_u-1A_g}\|$.

size remains approximately constant (that is, the resonance becomes stabilized). This is clearly illustrated by the decrease in the $\langle R^2 \rangle$ value. Since the matrix representation of R^2 does not depend on the CAP strength, $\langle R^2 \rangle$ is perfectly correlated with $\|\gamma\|$. On the other hand, the one-electron part of the total energy (and, in particular, the perturbation due to the CAP) depends on γ. Thus, eq 16 tells one that the energy perturbation due to the CAP is proportional to $\|\gamma\|$ giving rise to the linear dependence of the energy as a function of the CAP strength in the asymptotic region. These simple observations have led to a deperturbative correction that improved the robustness of CAP-augmented methods.[24,43]

It is important to distinguish the situations in which eq 16 may provide useful qualitative (or even quantitative) insights from the cases when its application (although formally correct) is useless. One can employ eq 16 to investigate the effect of changes in molecular geometry on matrix elements between states changing their character upon these displacements, while the matrix representation of the operator representing the interstate property does not change much. For example, in refs 21−23 eq 16 was applied to quantify the degree of one-electron character (modulated by the mixing excitonic, multiexciton, and charge-resonance configurations) in the transitions between the states involved in singlet fission. Below, we consider three lowest electronic states of polyenes that change their character and mix with each other along various displacements. We also compute interstate properties in ethylene dimer,[40] a model system used to analyze the effect of chromophore orientation on the NAC in the context of singlet fission.[41] The key here is that the trends in the matrix elements are driven by the trends in the wave functions.

As an example of a situation when application of eq 16 does not provide useful information, consider calculations of transition dipole moments between the ground and excited electronic states within CIS or TDDFT/TDA formalisms. In this case, $\|\gamma\| = 1$ for all transitions, yet some states are bright and some dark, as dictated by the symmetry and the MOs involved in the transition (that is, cos α is different for different excited states). Another example of this sort would be the behavior of the transition dipole moment between the two lowest states of an ionized dimer along the interfragment distance (e.g., He_2^+). The two electronic states in this case preserve their character,[44] and the transition between them remains predominantly one-electron ($\|\gamma\| \approx 1$); however, the magnitude of the dipole moment increases linearly[44] along the stretching coordinate because of the obvious trend in μ.

III. COMPUTATIONAL DETAILS

Calculations were performed using several theoretical approaches. First, for octatetraene we employ the semiempirical PPP-FCI model (the Pariser−Parr−Pople π-approximation at the full configuration interaction level)[45] that enables quick exploratory calculations with a complete account for π-electron correlation. Calculations for butadiene and ethylene were performed using the complete active space self-consistent field (CASSCF) method.[46] CASSCF interstate properties were computed using full analytic formulation—that is, full expression for derivative coupling has been used,[30] including non-Hellman−Feynman terms, as given by eq 14. For comparison purposes, we also computed the Hellman−Feynman part of NAC for ethylene dimer (see the Supporting Information (SI)); the differences between the two quantities are rather small and all trends are the same. In addition, RAS-2SF (restricted active space double spin-flip) calculations[47−49] were performed for ethylene dimer. Only singlet states were considered in this work.

dx.doi.org/10.1021/jp506090g | J. Phys. Chem. A 2014, 118, 11943−11955

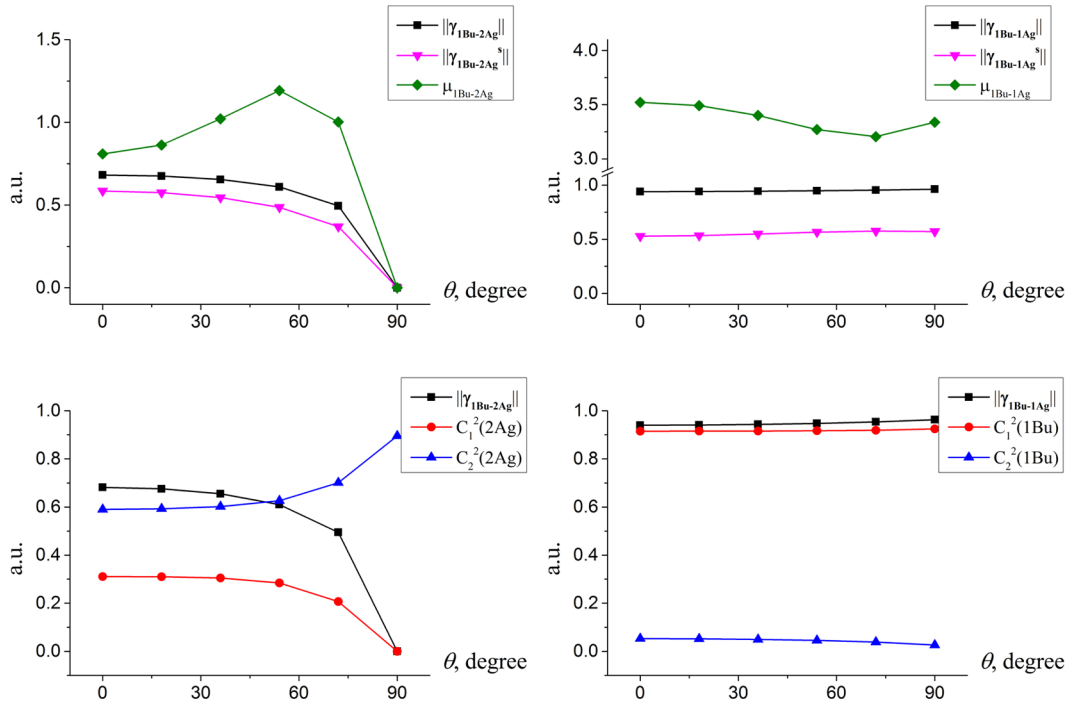

Figure 2. Top: Matrix elements of the dipole operator (a.u.) and $\|\gamma\|$ between the $2A_g/1B_u$ (left) and $1A_g/1B_u$ (right) states in octatetraene along twisting angle θ. Bottom: Weights of singly (C_1^2) and doubly (C_2^2) excited configurations in the wave functions of the $1B_u$ and $2A_g$ states.

The PPP-FCI calculations were performed using the conventional π-parametrization scheme.[50] The alternation in core integrals (resonance integrals) $\beta_{\mu\mu+1}$ in the *trans*-octatetraene chain and other π-parameters are the same as in ref 51. The simplified geometry for the carbon backbone is used (in the equilibrium configuration all CC bonds are of the same length 1.4 Å and all C−C−C angles equal 120°). We employed the FCI matrix algorithm from ref 52 implemented as Matematica notebooks.

RAS-2SF and CASSCF calculations of ethylene dimer used the 4-electrons-in-4-orbitals active space and the 6-31G* basis set. An active space of 4-electrons-in-4-orbitals was also used in the CASSCF calculations of butadiene. The CASSCF calculations were state-averaged with four states included in the average for both butadiene and ethylene dimer. The four singlet states included in the average are the states of importance here: the ground state, two excitonic states derived from the $\pi\pi^*$ excitation, and the doubly excited (ME) state. RAS-2SF calculations used a high-spin ROHF quintet reference.

The structure of the ethylene molecule was optimized at the RI-MP2/cc-pVTZ level of theory. Then the stacked dimer was constructed for the two identical monomers 3.5 Å apart. This structure was used as a starting point to generate displacements along the long and short axes.

CASSCF calculations were performed by Columbus.[53,54] RAS-2SF calculations were performed with Q-Chem.[55,56]

All relevant geometries are given in the SI.

IV. RESULTS AND DISCUSSION

We begin by considering polyenes, whose electronic structure is somewhat similar to that encountered in singlet fission systems. In all-trans polyenes, the two lowest excited states are of the A_g and B_u symmetry. At equilibrium geometry, the former has predominantly double-excited character, $(\pi^*)^2$, with respect to the ground state, $(\pi)^2$, and is dark, whereas the latter is dominated by a one-electron transition, $\pi\pi^*$, and is bright; $2A_g$ and ^1B_u are connected by a one-electron excitation. Changing molecular geometry modifies the character of these states thus affecting interstate properties such as transition dipole moments and NACs. We consider the interstate properties between the two exited states ($2A_g$ and $1B_u$), as well as between the ground $1A_g$ and the two excited states.

A. Octatetraene. Our first example is octatetraene. We consider two types of displacements—stretching the C4−C5 bond (symmetry-preserving) and twisting around C4−C5. Changes in the states' characters can be characterized by relative weights of the reference, singly, and doubly excited configurations.

Figure 1 shows the results for stretching along the C4−C5 bond obtained with the PPP-FCI model (see section III). Bond stretching parameter ζ is defined as $\zeta = r/r_e$, where r_e is the equilibrium bond length. We observe that the stretch has a very little effect on the $1A_g-1B_u$ transition dipole moment, while the $2A_g-1B_u$ transition dipole first increases from 0.8 to 1.1 and then monotonically drops to zero. This different behavior can be explained by the changes in the underlying wave functions. The ground-state wave function is dominated by the reference determinant at all values of ζ (e.g., at $\zeta = 1.5$, the weight of the reference is 0.88). Likewise, $1B_u$ retains its singly excited character. However, in the $2A_g$ state, the weight of doubly excited configurations increases from 0.6 to 0.9. This explains different trends in the respective μ_{tr}. We note that $\|\gamma\|$ catches the overall trend very well—it remains approximately constant for the $1A_g-1B_u$ transition and monotonically declines for $2A_g-1B_u$. However, finer variations in μ_{tr} (e.g., the initial ~25% rise) are not reproduced by $\|\gamma\|$. These variations arise because $\|\mu\|$ is not constant along these displacements; a simple analysis of the respective matrix elements reveals that $\|\mu\|$ increases linearly with the bond stretch (in the AO basis, the

dx.doi.org/10.1021/jp506090g | J. Phys. Chem. A 2014, 118, 11943−11955

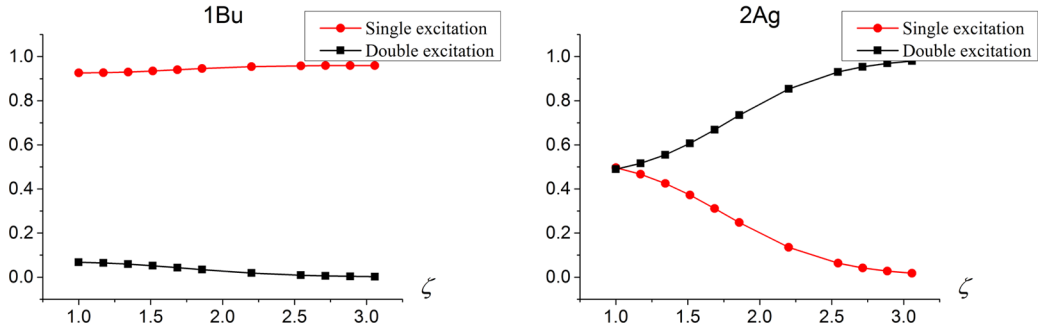

Figure 3. Weights of singly and doubly excited configurations in the wave functions of the $1B_u$ and $2A_g$ states of butadiene along the bond-stretching coordinate.

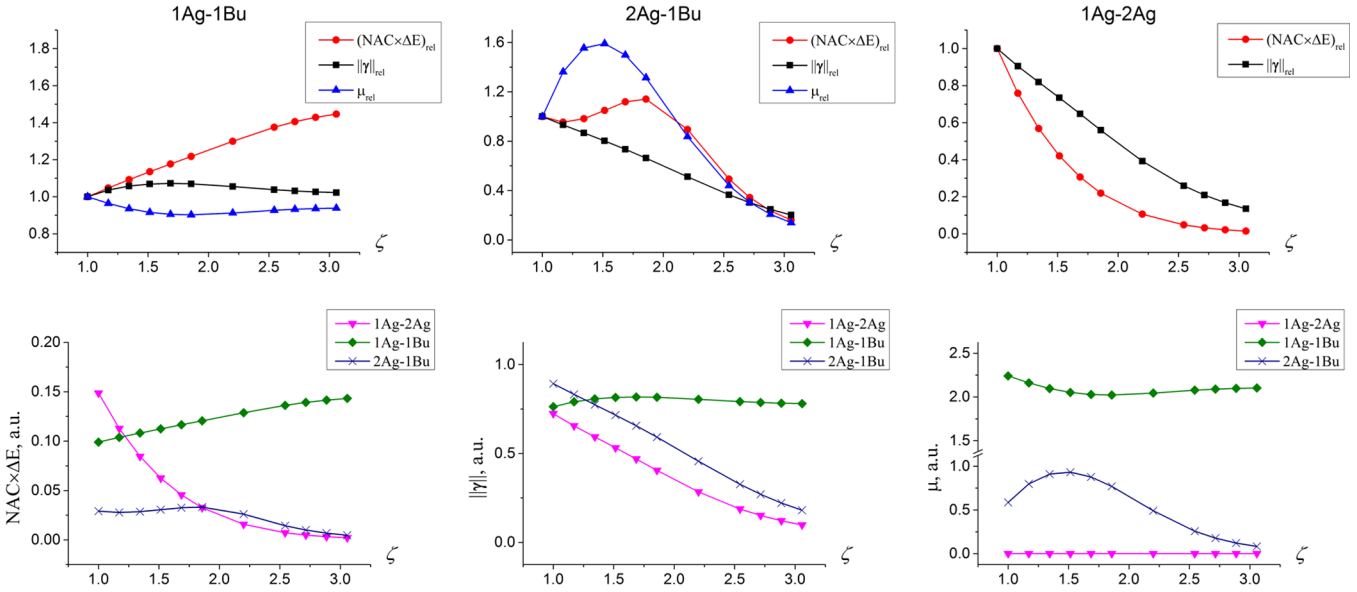

Figure 4. $\|\gamma\|$, μ and $\|\mathrm{NAC}\|\cdot\Delta E$ for the $1A_g-1B_u$ (left), $2A_g-1B_u$ (middle), and $1A_g-2A_g$ (right) transitions along the C2−C3 stretching coordinate in butadiene. Top: All quantities are normalized to their equilibrium ($\zeta = 1$) values. Bottom: Absolute values.

matrix of $\hat{\mu}$ is diagonally dominant with the matrix elements being roughly proportional to the Cartesian coordinates of the respective atoms).

We note that $\|\gamma\|$ and $\|\gamma^s\|$ behave similarly. $\|\gamma^s\|$ is about a factor of 2 smaller than the norm of unsymmetrized γ ($\|\gamma^s\| \leq \|\gamma\|$, by virtue of eq 8). $1B_u-1A_g$ transition, whereas for $1B_u-2A_g$, the values of the two norms are close. The trends are well reproduced by either symmetrized or unsymmetrized γ, since the two quantities parallel each other.

The behavior along the twisting coordinate is shown in Figure 2. Twisting lowers the symmetry (from C_{2h} to C_2) and the electronic states, strictly speaking, should not be labeled as A_g/B_u at twisted geometries (but A/B). However, since the state character changes smoothly (as evidenced by the wave function coefficients), we use these labels for clarity. As in the preceding example, the $1A_g$ and B_u states retain their characters along the torsional coordinate, whereas the $2A_g$ state eventually becomes doubly excited (at $\theta > 80°$). The trends in $\|\gamma\|$ follow the trends in wave function composition—for $1A_g-1B_u$, $\|\gamma\|$ is nearly constant, whereas for $2A_g-1B_u$, the value of $\|\gamma\|$ begins to decrease at about 60° reaching zero at 90°. As in the bond stretching example, the significant changes in μ_{tr} follow the trends in $\|\gamma\|$ (i.e., nearly constant value of μ_{tr} for $1A_g-1B_u$ and an eventual drop to zero for $2A_g-1B_u$); however, finer details, such as initial increase for the $2A_g-1B_u$ transition are due to the changes in $\|\mu\|$ and are not captured by $\|\gamma\|$. Specifically, the twist leads to the increase of $\|\mu\|$ because the extent of the molecule increases in the dimension perpendicular to the molecular plane (and because the symmetry is lowered); thus, for small twisting angles when $\|\gamma\|$ remains nearly constant, μ_{tr} shows initial rise (which is eventually overcome by the decline in $\|\gamma\|$ at large values of θ).

B. Butadiene. Our second example is butadiene where we consider OPDMs and interstate properties computed using the CASSCF wave functions.

We begin by considering the stretching along the central bond. The trends in the CASSCF wave functions of the three states are very similar to the octatetraene example. Figure 3 shows the weights of single and double amplitudes in the two excited states, $1B_u$ and $2A_g$ (the weights are defined relative to the reference Hartree−Fock determinant). The $1A_g$ state remains predominantly single-configurational (the weight of the reference is ≥0.9). As one can see, the $1B_u$ state remains singly excited with respect to the reference, whereas $2A_g$ becomes doubly excited.

These changes in the wave functions result in the following trends in $\|\gamma\|$: for the $1A_g-1B_u$ transition, $\|\gamma\|$ remains constant, whereas, for the $1A_g-2A_g$ and $2A_g-1B_u$ transitions, $\|\gamma\|$ decreases from approximately 1 to 0. The respective interstate matrix elements (μ_{tr} and $\|\mathrm{NAC}\|\cdot\Delta E$) follow this

dx.doi.org/10.1021/jp506090g | J. Phys. Chem. A 2014, 118, 11943−11955

trend, as illustrated in Figure 4. As in the octatetraene example, the correlation is not perfect and some fine variations are not reproduced by $\|\gamma\|$; however, the overall picture is correct—$1A_g-1B_u$ properties do not change along this displacement, whereas interstate properties for the $2A_g-1B_u$ and $1A_g-2A_g$ transitions significantly decrease. Nonmonotonic behavior of the actual matrix elements is due to the variations in the respective matrix representations of the dipole moment and derivative operators. The changes in the dipole moment matrix along stretching and twisting coordinates is explained above. The reason behind variations of the derivative matrix elements, eq 12, is different; it is analyzed in detail in the next section.

The behavior along the twisting coordinate is also similar to octatetraene; the results are shown in SI.

C. Ethylene Dimer. Motivated by singlet fission, we now proceed to the ethylene dimer,[40] a model system used to investigate the effect of relative chromophore orientation on the electronic couplings.[41]

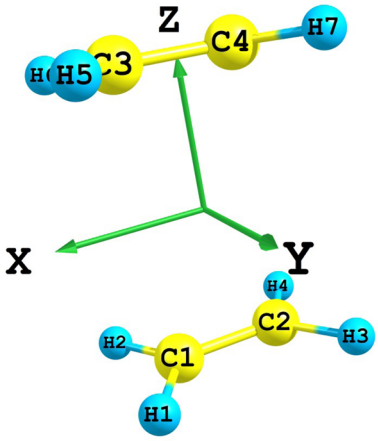

Figure 5. Ethylene dimer at $Z = 3.5$ Å and $X = Y = 0$.

The dimer geometry is shown in Figure 5. Figure 6 shows $\|\gamma\|$ computed by RAS-2SF as a function of the displacements along X and Y coordinates defined in Figure 5. At the displaced geometries ($X \neq 0$ and $Y \neq 0$), the symmetry of the system is C_i. We consider the following states: the ground state, the doubly excited state that is similar to the ^{1}ME states in acenes (two local $^3\pi\pi^*$ excitations coupled into a singlet), and two states derived from local $\pi\pi^*$ excitations that are similar to the S_1 and $S_{1'}$ states in the context of singlet fission.[21] The ground, ME, and S_1 states are *gerade*; $S_{1'}$ is *ungerade*. The RAS-2SF active space orbitals and their symmetries are shown in the SI. In the CASSCF calculations, we analyze both S_1 and $S_{1'}$; however, in RAS-2SF scheme only the former can be computed reliably (because $S_{1'}$ lies relatively high in energy and includes significant contributions of hole configurations).

As one can see, the magnitude of $\|\gamma\|$ at the perfectly stacked geometry ($X = Y = 0$) is nonzero. The displacement along Y leads to the monotonic decrease, whereas the trend along X is more complicated—we first observe an increase in $\|\gamma\|$ that reaches maximum at about 0.6 Å, which is approximately half of the carbon−carbon bond length (1.33 Å).

These variation in $\|\gamma\|$ can be tracked down to varying weights of the charge-resonance (CR) terms in the S_1 wave function. The configuration analysis at the selected geometries is given in SI and is summarized in Table 1 (see also Appendix C).

Table 1. Configuration Analysis of the RAS-2SF Wave Functions of the ME and S_1 States Using Localized Orbitals within DMO-LCFMO Framework[a]

state	X(Å)	Y(Å)	ME	CR	EX
^{1}ME	0	0	0.98	0.02	0.00
	0.8	0	0.92	0.04	0.03
	0	2	1.00	0.00	0.00
S_1	0	0	0.00	0.66	0.26
	0.8	0	0.00	0.70	0.17
	0	2	0.00	0.06	0.86

[a]See ref.[21]

We observe that the ^{5}ME state retains its pure multiexciton character (TT). The ^{1}ME state shows small amount (2−4%) of CR at perfectly stacked ($X = Y = 0$) and slightly displaced (along X) geometries. The character of S_1 state varies more considerably. At strongly displaced geometries (e.g., $Y = 2$ Å, $X = 0$), the S_1 state is almost pure excitonic (the weight of CR is 6%); however, at small displacements, the CR configurations become dominant (~70%). An increase in $\|\gamma\|$ at small displacements along the long axis ($Y = 0$) clearly correlates with a slight increase of the CR weight in S_1. Interestingly, this behavior is different from the trends observed in ref 23, where it was found that favorable couplings in certain polymorph structures arise mostly due to the admixture of CR configurations into the ^{1}ME state, while S_1 remains purely excitonic.

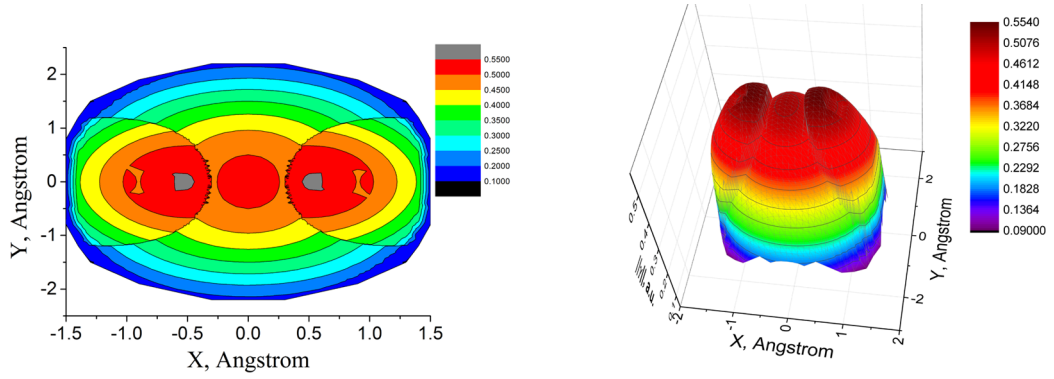

Figure 6. $\|\gamma\|$ for the ^{1}ME−S_1 states as a function of the displacements along the long (X) and short (Y) axes.

dx.doi.org/10.1021/jp506090g | J. Phys. Chem. A 2014, 118, 11943−11955

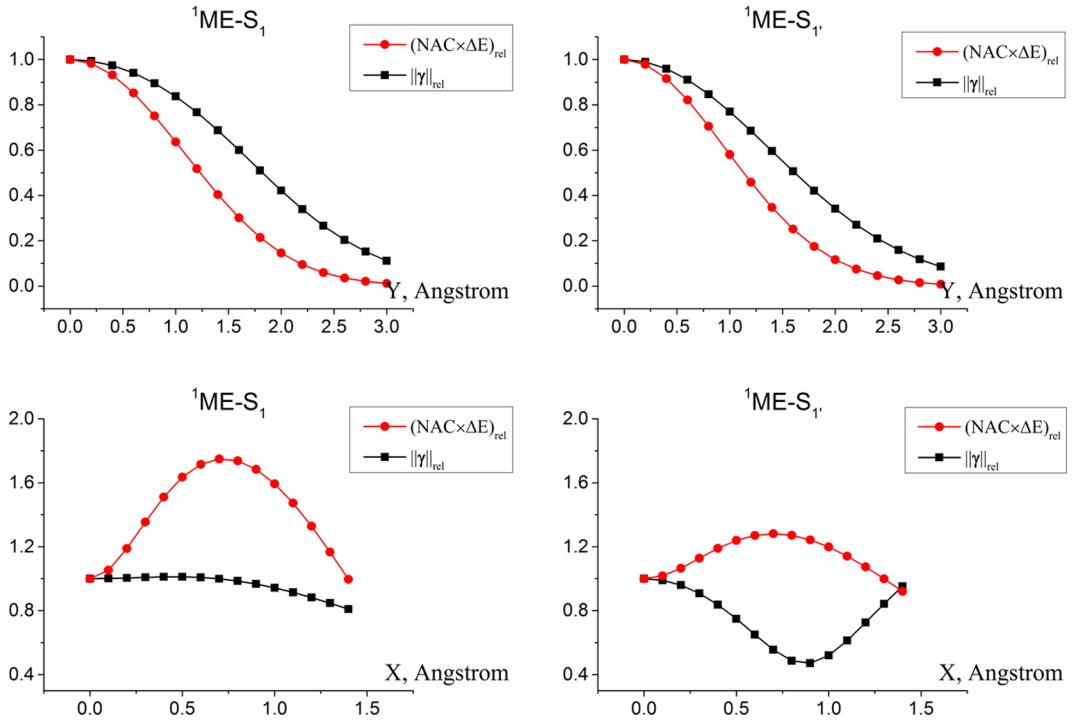

Figure 7. $\|\gamma\|$ and interstate properties for the ME−S_1 (left) and ME−$S_{1'}$ (right) transitions computed using CASSCF.

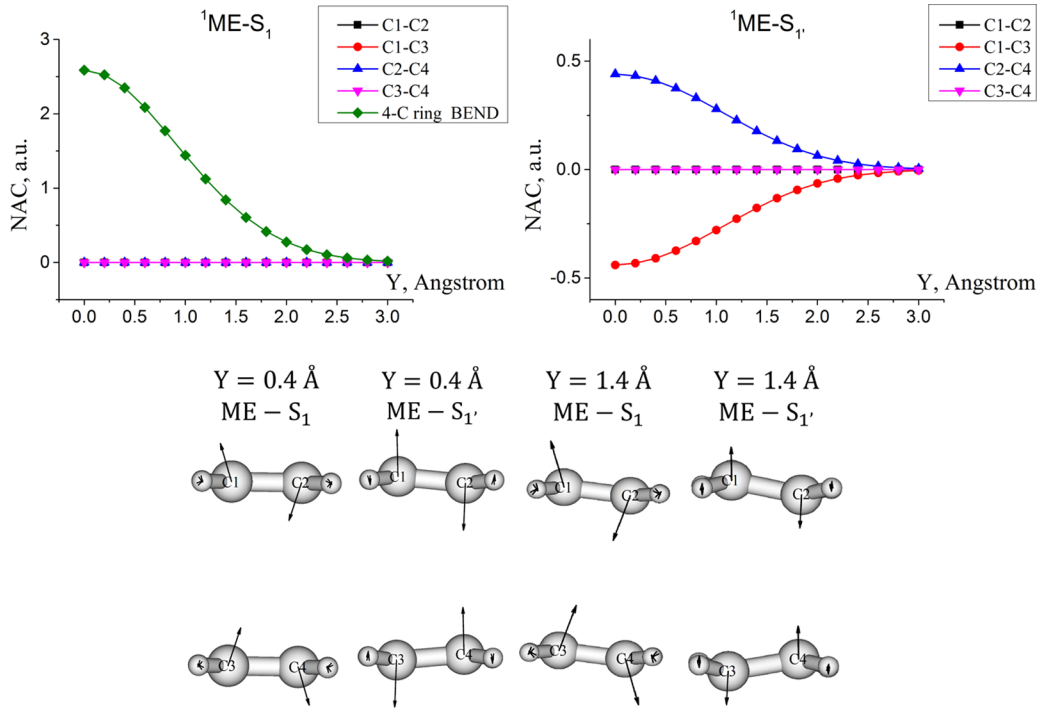

Figure 8. Leading components of NAC along the $X = 0$ scan for the ME−S_1 (left) and ME−$S_{1'}$ (right) transitions.

Figure 7 shows the CASSCF couplings between the ME−S_1 and ME−$S_{1'}$ states and $\|\gamma\|$ along the two cuts (all values are normalized to their respective values at $X = Y = 0$). For the displacement along the short axis (X = 0 cut), we observe a nearly perfect correlation between $\|\text{NAC}\|\cdot\Delta E$ and $\|\gamma\|$; however, the behavior along the $Y = 0$ cut is more complex. $\|\gamma\|$ shows relatively small variations, and so does NAC. The fine details, however, are not reproduced. For example, for the ME−S_1 pair (right panel of Figure 6), NAC shows up to a 1.6 times increase at the displaced geometries, whereas $\|\gamma\|$ remains nearly constant. We note that the difference between the Hellman−Feynman part and the full NAC is very small, as illustrated for the $Y = 0$ cut in the SI.

To better understand these trends, we consider the individual components of NAC along the $X = 0$ (Figure 8) and $Y = 0$ (Figure 9) scans. The NAC vector can be described as intra- and intermolecular carbon−carbon displacements; the leading components are shown in Figures 8 and 9. We observe that, for

dx.doi.org/10.1021/jp506090g | J. Phys. Chem. A 2014, 118, 11943−11955

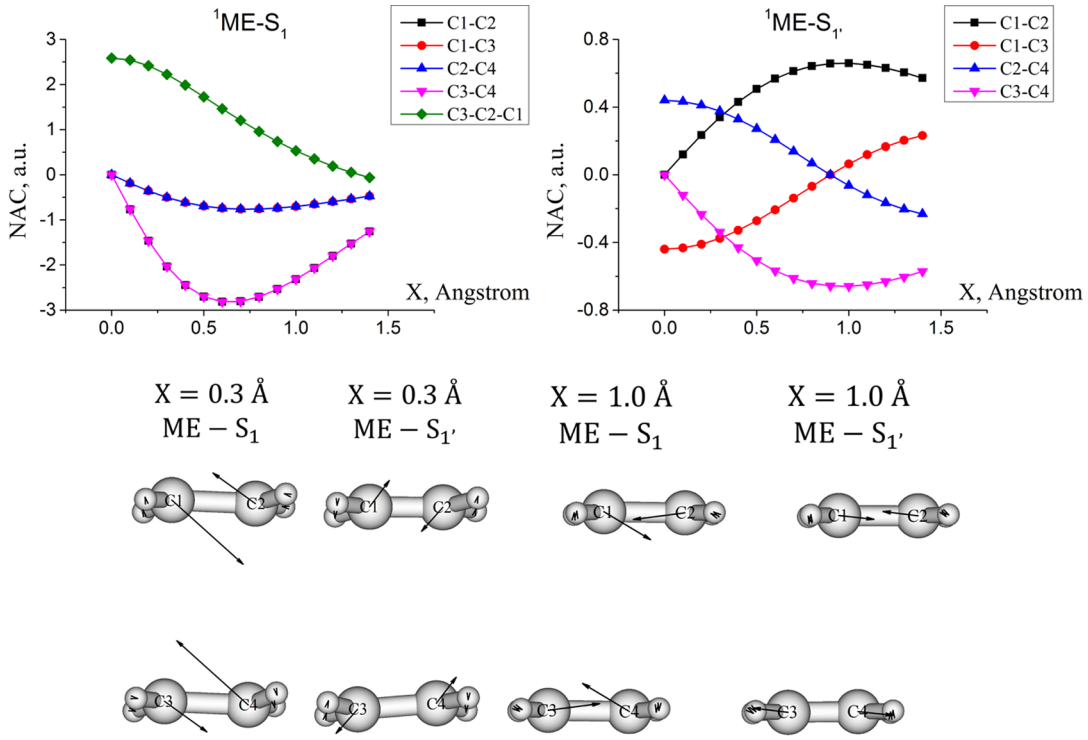

Figure 9. Leading components of NAC along the $Y = 0$ scan for the ME−S_1 (left) and ME−$S_{1'}$ (right) transitions.

the $X = 0$ scan, intramolecular components of NAC are zero and that the trends in intermolecular components follow the trends in γ. However, along the $Y = 0$ scan, both intra- and intermolecular components are nonzero and the former does not follow $\|\gamma\|$. For example, for the ME−$S_{1'}$ pair, the intermolecular NAC components (C1−C3 and C2−C4) follow the trends in $\|\gamma\|$ closely showing the initial decrease (in absolute values) up to ≈0.7 Å followed by an increase. However, intramolecular components (C1−C2 and C3−C4) are exactly zero at the perfectly stacked configuration but rise sharply and become dominant at large X; they remain nearly constant after the initial rise. Since the absolute value of NAC, ||NAC||, is a sum of all components, the trends due to the change in the states characters (that define intermolecular components) become obscured. The couplings for the ME−S_1 pair (along $Y = 0$) show a similar trend—the intermolecular components are nearly constant (as are $\|\gamma\|$), whereas intramolecular ones exhibit a maximum and have larger values. Thus, the discrepancy between the trends in $\|\gamma\|$ and the actual NAC can be attributed to a more complex behavior of the intramolecular components of NACs.

The difference in behavior of intra- and intermolecular components can be rationalized by considering the explicit form of the coupling operator from eq 11 that is given by eq 12. Thus, the contribution to NAC due to displacements of atom A along x_A is

$$\frac{\partial}{\partial x_A}\hat{V}_{\text{en}} = -\sum_i \frac{Z_A \cdot \text{sign}(R_A - r_i)}{(R_A - r_i)^2} \tag{19}$$

Consequently, for any symmetric vibration of two symmetry-equivalent atoms, such as, for example, C1C2 bond stretch (in which the two carbons move in opposite directions) at $X = 0$, the respective terms cancel out. This is further illustrated in Figure S7 (see the SI) that shows Cartesian components of NAC along the two scans. That is why C1C2 and C3C4 NAC components are exactly zero along the $X = 0$ scan. We note that vibrations in which both carbons are moving in the same direction (thus keeping the CC bond length constant) are expected to cause smaller perturbations in the wave functions and, consequently, smaller contributions to NACs. However, when the two carbons become inequivalent (such as at $X \neq 0$; see Figure S7 of the SI), the two derivatives do not cancel out giving rise to nonzero NAC. This explains the observed rise of intramolecular components of NACs along the $Y = 0$ scan. These observations can be generalized as follows:

(1) Intramolecular components of NACs along symmetric vibrations are expected to be large, provided that the atoms involved have a different local environment.

(2) Dimer calculations may be insufficient to quantify intramolecular components; e.g., the local environment in a periodic solid might differ from that in the dimer.

(3) Intramolecular components depend strongly on relative orientation of the fragments; this dependence is driven by the trends in $\nabla_R \hat{V}_{\text{en}}$ and, therefore, it does not always follow the trends in $\|\gamma\|$. For example, they can show large variations even when $\|\gamma\| \approx$ const.

(4) Intermolecular components follow the trends in $\|\gamma\|$ very well. Their magnitude can be as large as that of the intramolecular components.

In the context of SF, an important question is whether intra- or intermolecular components are more important for the overall rate of nonadiabatic transitions. To answer this question, one needs to evaluate the rate. As discussed in the Appendix, the total rate depends on both the coupling and the nuclear momentum. Thus, the components of Franck−Condon displacements will have a crucial effect on the overall coupling. For example, if the initially excited state (e.g., S_1 in SF) has large displacements along intermolecular coordinates, the rate will be driven by the intermolecular NACs. Thus, in order to

dx.doi.org/10.1021/jp506090g | J. Phys. Chem. A 2014, 118, 11943−11955

fully understand the effect of morphology on the SF rates, one needs to consider Franck−Condon displacements, in addition to the NACs, and evaluate rates using models that take both these factors into account (such as in refs 57 and 58). We stress, however, that regardless of whether inter- or intramolecular couplings play a major role, one needs to have large $\|\gamma\|$ in order to have large couplings (that is, large $\|\gamma\|$ is necessary but not sufficient).

V. CONCLUSION

In this work, we investigated the utility of the norms of OPDMs for evaluating the trends in state and interstate properties. By comparing full calculations of transition dipole moments and NACs with $\|\gamma\|$ for selected model systems, we illustrate that while variations of $\|\gamma\|$ do contribute systematically to the total matrix elements (e.g., when $\|\gamma\| = 0$, then the respective matrix element of a one-electron operator is also zero), the finer details might not be reproduced because the magnitude of the operator might also vary giving rise to a more complex trend. Analysis of NACs computed for a model singlet fission system, ethylene dimer, reveals that intermolecular components of NACs follow the trends in $\|\gamma\|$ well, as they are determined primarily by the characters of the two wave functions; however, intramolecular components depend on the relative orientation of the two moieties via the dependence in $(\partial \hat{V}_{en}/\partial R)$. Therefore, intramolecular NACs can exhibit large variations even when changes in $\|\gamma\|$ are small. In other words, large values of $\|\gamma\|$ are necessary but not sufficient for maximizing the couplings. For ethylene dimer, we observe large NACs at perfectly stacked geometry, contrary to the predictions derived based on model Hamiltonians.[40] However, larger values (by a factor of 1.6) are indeed observed at slip-stacked (along the long axis) geometries, in agreement with the predictions of Michl and coworkers.[40] Larger values of NACs at slip-stacked configurations are due to the breaking of symmetry of the local environments of the heavy atoms and not due to the wave function composition. The variations in $\|\gamma\|$ for ethylene dimer are due to a varying admixture of the CR configurations to the S_1 state, whereas the ^{1}ME state retains its pure multiexciton character. This is different from the trends observed in ref 23, where it was found that favorable couplings arise mostly due to the admixture of CR configurations into the ^{1}ME state.

In sum, $\|\gamma\|$ provides a useful tool for analyzing the trends in couplings; however, for quantitative calculations full derivative coupling is desirable. In order to fully understand the effect of morphology on the rates of nonadiabatic transitions in molecular solids, one needs to employ models that take into account which nuclear motions are activated by electronic excitations.

APPENDIX A. SUM RULES FOR TRANSITION DENSITY MATRICES

In this section we discuss some properties of transition OPDMs defined by eq 4. We employ an orthonormal spin−orbital basis of size M; the number of electrons is N.

When the initial and final states coincide, γ becomes regular OPDM defined by eq 2; its trace equals N owing to the normalization condition. For transition DMs

$$\mathrm{Tr}[\gamma^{if}] = 0 \tag{20}$$

To derive properties of $\|\gamma^{if}\|^2$, we begin by defining the following spectral sum:

$$S[i] = \sum_f \|\gamma^{if}\|^2 \tag{21}$$

where sum runs over all electronic states of the system. Using eqs 4 and 7,

$$\begin{aligned} S[i] &= \sum_f \sum_{pq} (\gamma_{pq}^{if})^2 \\ &= \sum_{pq} \sum_f \langle \Psi_i | p^+ q | \Psi_f \rangle \langle \Psi_f | q^+ p | \Psi_i \rangle \\ &= \sum_{pq} \langle \Psi_i | p^+ q q^+ p | \Psi_i \rangle \end{aligned} \tag{22}$$

where the last step exploits resolution-of-the-identity $\hat{1} = \sum_f |\Psi_f\rangle\langle\Psi_f|$.

Using commutator rules for creation and annihilation operators, eq 22 can be rewritten as

$$S[i] = \sum_p \langle \Psi_i | p^+ p | \Psi_i \rangle - \sum_p \langle \Psi_i | p^+ \hat{N} p | \Psi_i \rangle \tag{23}$$

where $\hat{N}$ is the number operator, $\hat{N} = \sum_p p^+ p$, which satisfies the following properties:

$$\hat{N}|\Psi\rangle = N|\Psi\rangle \tag{24}$$

$$\hat{N} p |\Psi\rangle = (N-1)|\Psi\rangle \tag{25}$$

Then, we arrive at the final result:

$$\sum_f \|\gamma^{if}\|^2 = N(M - N + 1) \tag{26}$$

This sum rule can be used, for example, to test the correctness of OPDMs within FCI. We note that this expression is only valid when all excited states are included in the sum; however, it is also trivially satisfied for the CIS model (when the initial state is the Hartree−Fock reference state).

It is convenient to rewrite eq 26 as follows:

$$\sum_{f \neq i} \|\gamma^{if}\|^2 = N(M - N) + N - \mathrm{Tr}[(\gamma^{ii})^2] \tag{27}$$

If the initial state is chosen to be the ground state, then the above sum runs over all excited states of the system. In a sense, eq 27 provides an average measure of all one-electron interactions between the ground and all excited states of the system.

Equation 27 can be rewritten as

$$\sum_{f \neq i} \|\gamma^{if}\|^2 = N(M - N) + N_{odd}/2 \tag{28}$$

where N_{odd} is the effective number of unpaired electrons as given by the Yamaguchi-like index:[10]

$$N_{odd} \equiv 2(N - \mathrm{Tr}[(\gamma^{ii})^2]) \tag{29}$$

We note that eq 29 will give zero for a single maximum spin-projection determinant and can only be used to compute the number of unpaired electrons due to correlation. Because $N_{odd} = 0$ for single-determinantal wave functions, one can see that it can be thought of as an average measure of of correlation effects in one-electron transition properties. Recall that $N\cdot(M - N)$ is the total number of the CIS excited states, that is, the number of the singly excited determinants from the reference determinant.

We also note that $N\cdot(M - N) = N_{occ}N_{virt}$ and, therefore, is equal to the total number of singly excited states in a general (non-CIS) calculation. For closed-shell molecules whose ground-state wave function is dominated by a single determinant, $N_{odd} \ll N$. Thus, one can expect that for a given molecule $\sum_{f\neq i}\|\gamma^{if}\|^2$ should be close to the respective CIS value regardless of the electronic structure model.

Sum rule (26) can be also inferred from more general relations derived in ref 59. In particular, for transition OPDMs one can prove the following matrix identities:

$$\sum_f \gamma^{if}(\gamma^{if})^+ = (M - N + 1)\gamma^{ii} \tag{30}$$

$$\sum_g \gamma^{ig}(\gamma^{gf})^+ = (M - N + 1)\gamma^{if} \tag{31}$$

Analogous relations can be obtained for many-particle DMs.

APPENDIX B. NONADIABATIC COUPLINGS AND RATES OF NONADIABATIC TRANSITIONS

A rate of nonadiabatic transition between the initial i and final f electronic states of the system is given by the Fermi Golden Rule (derived for the thermally averaged rate within the first-order PT):

$$k_{i\to f} = 2\pi\langle\sum_{f'}|\langle\Phi_i\xi_{i'}|T_n|\Phi_f\xi_{f'}\rangle|^2\delta(E_{ii'} - E_{ff'})\rangle_T \tag{32}$$

where $\Phi_i\xi_{i'}$ and $\Phi_f\xi_{f'}$ denote the initial and final states, the sum runs over the final vibrational states, and the thermal averaging over the initial vibrational states is performed. $E_{ii'}$ and $E_{ff'}$ denote total (electronic and nuclear) energies of the initial and final states. Depending on the physics of the problem, different approximations to this expression are possible.[57,58,60]

As discussed in refs 60 and 61, a classical approximation to eq 32 can be written as

$$k_{i\to f} = 2\pi\langle|\sum_A -\frac{i}{M_A} < \Phi_i|\nabla_A\Phi_f > p_A|^2\delta(E_{ii'} - E_{ff'})\rangle_T \tag{33}$$

where p_A is a classical momentum along the nuclear coordinate A. Equation 33 clearly illustrates the importance of nuclear motions. It is nuclear kinetic energy that closes the electronic gap. Likewise, in surface hopping simulations, total energy conservation is enforced by scaling the nuclear momentum to compensate for electronic level mismatch, $U_i - U_f$. Averaging over initial and final vibrational states takes into account density of states available for the system.

Nuclear motions and, consequently, calculations of the thermal averaging in eq 33, depend on the initial conditions and interactions of the system with the bath. In the context of the present work, the important result is that the rate of the nonadiabatic transition is proportional to $\|\langle\Psi_i|\nabla|\Psi_f\rangle\|^2$, or, in virtue of eq 16, to $[\|\gamma\|/(U_i - U_f)]^2$. While this expression cannot be used to predict absolute rates of nonadiabatic transitions, it can be exploited to explain general trends, as was done in ref 22 and 23.

APPENDIX C. ANALYSIS OF THE MULTIEXCITON WAVE FUNCTIONS

Here we discuss a 4-electron-in-4-orbital representation of the ME wave functions. Consider a dimer, such as a stacked ethylene dimer. Assuming localized orbitals, h_A, l_A, h_B, and l_B, where A and B denote the two fragments, the ME wave functions can be derived by appropriately spin-adapting the following electronic configuration in which both fragments are excited: $|h_Al_Ah_Bl_B\rangle$. To obtain ^{1}ME, one can start with the $|\alpha\alpha\beta\beta\rangle$ determinant with the above orbital occupation and apply an appropriate Löwdin projector, $\hat{O}_{S=0}$. This leads to the following normalized spin-pure function:[2]

$$\begin{aligned}|^1\mathrm{ME}\rangle &= \sqrt{3}\,\hat{O}_{S=0}|\alpha\alpha\beta\beta\rangle \\ &= \frac{1}{2\sqrt{3}}(2|\alpha\alpha\beta\beta\rangle + 2|\beta\beta\alpha\alpha\rangle - |\alpha\beta\alpha\beta\rangle - |\beta\alpha\beta\alpha\rangle \\ &\quad - |\alpha\beta\beta\alpha\rangle - |\beta\alpha\alpha\beta\rangle)\end{aligned} \tag{34}$$

Analogously, the quintet $M_S = 0$ component is

$$\begin{aligned}|^5\mathrm{ME}\rangle &= \sqrt{6}\,\hat{O}_{S=2}|\alpha\alpha\beta\beta\rangle \\ &= \frac{1}{\sqrt{6}}(|\alpha\alpha\beta\beta\rangle + |\beta\beta\alpha\alpha\rangle + |\alpha\beta\alpha\beta\rangle + |\beta\alpha\beta\alpha\rangle \\ &\quad + |\alpha\beta\beta\alpha\rangle + |\beta\alpha\alpha\beta\rangle)\end{aligned} \tag{35}$$

The FCI/PPP calculations of the stacked ethylene dimer (at Z = 4 Å) yield expansion coefficients that are almost exactly equal to the above values, i.e., $1/\sqrt{12} \approx 0.28867$, $1/\sqrt{3} \approx 0.57735$, and $1/\sqrt{6} \approx 0.40825$. The spin-flip formulation of FCI yields a configurational expansion identical to the conventional one; the differences in signs can be reconciled by properly rearranging the indices (see eq (4.24) from ref 62). Consequently, RAS-2SF amplitudes from Tables S1−S4 of the SI are also close to these values. This is because the ME states at these configurations do not show noticeable couplings with the CR configurations and retain their pure TT character (see Table 1).

We also note that the ME state can be identified by a calculation of the local spin,[63] $\langle S^2\rangle$, of the monomers. By applying the technique from ref 64 to the PPP-FCI wave functions, we find that $\langle S^2\rangle_A = \langle S^2\rangle_B \approx 2$, while the total $\langle S^2\rangle_{AB}$ is, of course, zero. Such local spin calculations provide a useful diagnostic for identifying ME states in more complex systems.

ASSOCIATED CONTENT

Supporting Information

Figures showing CASSCF interstate properties for butadiene; RAS-2SF and CASSCF potential energies, Cartesian components of NAC, HOMO and LUMO, and additional data along X = 0 and Y = 0 scans for ethylene dimer; tables with wave function analysis and relevant Cartesian geometries. This material is available free of charge via the Internet at http://pubs.acs.org.

AUTHOR INFORMATION

Notes

The authors declare no competing financial interest.

ACKNOWLEDGMENTS

We are grateful to Prof. M. M. Mestechkin for his feedback regarding the manuscript. This material is based upon work supported by the Center for Energy Nanoscience, an Energy Frontier Research Center funded by the U.S. Department of Energy, Office of Science, Office of Basic Energy Sciences (Grant DE-SC0001013) and by the DE-FG02-05ER15685 grant (A.I.K.). S.M. acknowledges support by the National Science Foundation (Grant CHE-1213614). A.I.K. and S.M.

gratefully acknowledge support from the Humboldt Foundation.

REFERENCES

(1) McWeeny, R. *Methods of Molecular Quantum Mechanics*, 2nd ed.; Academic Press: New York, 1992.
(2) Davidson, E. R. *Reduced Density Matrices in Quantum Chemistry*; Academic Press, New York, 1976.
(3) Mestechkin, M. M. *Metod matritsy plotnosti v teorii molekul*; Naukova Dumka, Kiev, Ukraine, 1977.
(4) Helgaker, T.; Jørgensen, P.; Olsen, J. *Molecular electronic structure theory*; John Wiley & Sons: New York, 2000.
(5) Equation 1 is also valid in a nonorthonormal AO basis if instead of A_{pq}, one makes use of contravariant matrix A^{pq}.
(6) Szabo, A.; Ostlund, N. S. *Modern Quantum Chemistry: Introduction to Advanced Electronic Structure Theory*; McGraw-Hill: New York, 1989.
(7) Bader, R. F. W. *Atoms in molecules—Quantum theory*; Oxford University Press: Oxford, U.K., 1990.
(8) Weinhold, F.; Landis, C. R. *Discovering Chemistry with Natural Bond Orbitals*; John Wiley & Sons, Hoboken, NJ, USA, 2012.
(9) Glendening, E. D.; Badenhoop, J. K.; Weinhold, F. Natural resonance theory: II. Natural bond order and valency. *J. Comput. Chem.* **1998**, *19*, 610−627.
(10) Takatsuka, K.; Fueno, T.; Yamaguchi, K. Distribution of odd electrons in ground-state molecules. *Theor. Chim. Acta* **1978**, *48*, 175−183.
(11) Head-Gordon, M. Characterizing unpaired electrons from the one-particle density matrix. *Chem. Phys. Lett.* **2003**, *372*, 508−511.
(12) Luzanov, A. V.; Prezhdo, O. V. Analysis of multiconfigurational wave functions in terms of hole-particle distributions. *J. Chem. Phys.* **2006**, *124*, No. 224109.
(13) Head-Gordon, M.; Grana, A. M.; Maurice, D.; White, C. A. Analysis of electronic transitions as the difference of electron attachment and detachment densities. *J. Phys. Chem.* **1995**, *99*, 14261−14270.
(14) Luzanov, A. V.; Zhikol, O. A. Electron invariants and excited state structural analysis for electronic transitions within CIS, RPA, and TDDFT models. *Int. J. Quantum Chem.* **2010**, *110*, 902−924.
(15) Luzanov, A. V.; Zhikol, O. A. In *Practical aspects of computational chemistry I: An overview of the last two decades and current trends*; Leszczynski, J., Shukla, M. K., Eds.; Springer: Berlin, 2012; p 415.
(16) Plasser, F.; Lischka, H. Analysis of excitonic and charge transfer interactions from quantum chemical calculations. *J. Chem. Theory Comput.* **2012**, *8*, 2777−2789.
(17) Bravaya, K.; Khrenova, M. G.; Grigorenko, B. L.; Nemukhin, A. V.; Krylov, A. I. The effect of protein environment on electronically excited and ionized states of the green fluorescent protein chromophore. *J. Phys. Chem. B* **2011**, *8*, 8296−8303.
(18) Luzanov, A. V. The structure of the electronic excitation of molecules in quantum-chemical models. *Russ. Chem. Rev.* **1980**, *49*, 1033−1048.
(19) Luzanov, A. V.; Sukhorukov, A. A.; Umanskii, V. E. Application of transition density matrix for analysis of excited states. *Theor. Exp. Chem.* **1976**, *10*, 354−361.
(20) Tretiak, S.; Mukamel, S. Density matrix analysis and simulation of electronic excitations in conjugated and aggregated molecules. *Chem. Rev.* **2002**, *102*, 3171−3212.
(21) Feng, X.; Luzanov, A. V.; Krylov, A. I. Fission of entangled spins: An electronic structure perspective. *J. Phys. Chem. Lett.* **2013**, *4*, 3845−3852.
(22) Kolomeisky, A. B.; Feng, X.; Krylov, A. I. A simple kinetic model for singlet fission: A role of electronic and entropic contributions to macroscopic rates. *J. Phys. Chem. C* **2014**, *118*, 5188−5195.
(23) Feng, X.; Kolomeisky, A. B.; Krylov, A. I. Dissecting the effect of morphology on the rates of singlet fission: Insights from theory. *J. Phys. Chem. C* **2014**, DOI: 10.1021/jp505942k.
(24) Jagau, T.-C.; Zuev, D.; Bravaya, K. B.; Epifanovsky, E.; Krylov, A. I. A fresh look at resonances and complex absorbing potentials: Density matrix based approach. *J. Phys. Chem. Lett.* **2014**, *5*, 310−315.
(25) Yarkony, D. R. Diabolical conical intersections. *Rev. Mod. Phys.* **1996**, *68*, 985−1013.
(26) Yarkony, D. R. Conical intersections: Diabolical and often misunderstood. *Acc. Chem. Res.* **1998**, *31*, 511−518.
(27) Yarkony, D. R. Conical intersections: The new conventional wisdom. *J. Phys. Chem. A* **2001**, *105*, 6277−6293.
(28) Lengsfield, B. H.; Saxe, P.; Yarkony, D. R. On the evaluation of nonadiabatic coupling matrix-elements using SA-MCSCF/CI wave functions and analytic gradient methods. 1. *J. Chem. Phys.* **1984**, *81*, 4549−4553.
(29) Saxe, P.; Lengsfield, B. H.; Yarkony, D. R. On the evaluation of non-adiabatic coupling matrix-elements for large-scale CI wave-functions. *Chem. Phys. Lett.* **1985**, *113*, 159−164.
(30) Lischka, H.; Dallos, M.; Szalay, P. G.; Yarkony, D. R.; Shepard, R. Analytic evaluation of nonadiabatic coupling terms at the MR-CI level. I. Formalism. *J. Chem. Phys.* **2004**, *120*, 7322−7329.
(31) Tapavicza, E.; Bellchambers, G. D.; Vincent, J. C.; Furche, F. *Ab initio* non-adiabatic molecular dynamics. *Phys. Chem. Chem. Phys.* **2013**, *15*, 18336−18348.
(32) Fatehi, S.; Alguire, E.; Shao, Y.; Subotnik, J. E. Analytic derivative couplings between configuration-interaction-singles states with built-in electron-translation factors for translational invariance. *J. Chem. Phys.* **2011**, *135*, No. 234105.
(33) Zhang, X.; Herbert, J. M. Analytic derivative couplings for spin-flip configuration interaction singles and spin-flip time-dependent density functional theory. *J. Chem. Phys.* **2014**, http://dx.doi.org/10.1063/1.4891984.
(34) Domcke, W. D., Yarkony, D. R., Köppel, H., Eds. *Conical intersections. Electronic structure, dynamics and spectroscopy*; World Scientific: Singapore, 2004.
(35) Helgaker, T.; Coriani, S.; Jørgensen, P.; Kristensen, K.; Olsen, J.; Ruud, K. Recent advances in wave function-based methods of molecular-property calculations. *Chem. Rev.* **2012**, *112*, 543−631.
(36) Lengsfield, B. H., III; Yarkony, D. R. Nonadiabatic interactions between potential energy surfaces: Theory and applications. *Adv. Chem. Phys.* **1992**, *82*, 1−72.
(37) Dallos, M.; Lischka, H.; Shepard, R.; Yarkony, D. R.; Szalay, P. G. Analytic evaluation of nonadiabatic coupling terms at the MR-CI level. II. Minima on the crossing seam: Formaldehyde and the photodimerization of ethylene. *J. Chem. Phys.* **2004**, *120*, 7330−7339.
(38) Ichino, T.; Gauss, J.; Stanton, J. F. Quasidiabatic states described by coupled-cluster theory. *J. Chem. Phys.* **2009**, *130*, No. 174105.
(39) Smith, M. B.; Michl, J. Singlet fission. *Chem. Rev.* **2010**, *110*, 6891−6936.
(40) Smith, M. B.; Michl, J. Recent advances in singlet fission. *Annu. Rev. Phys. Chem.* **2013**, *64*, 361−368.
(41) Johnson, J. C.; Nozik, A. J.; Michl, J. The role of chromophore coupling in singlet fission. *Acc. Chem. Res.* **2013**, *46*, 1290−1299.
(42) When treating an operator in a nonorthonormal AO basis, one should distinguish (as in tensor calculus) covariant, contravariant, and regular matrices of the operator. Within quantum chemistry context these peculiarities are discussed in ref 65.
(43) Zuev, D.; Jagau, T.-C.; Bravaya, K. B.; Epifanovsky, E.; Shao, Y.; Sundstrom, E.; Head-Gordon, M.; Krylov, A. I. Complex absorbing potentials within EOM-CC family of methods: Theory, implementation, and benchmarks. *J. Chem. Phys.* **2014**, *141*, No. 024102.
(44) Pieniazek, P. A.; Arnstein, S. A.; Bradforth, S. E.; Krylov, A. I.; Sherrill, C. D. Benchmark full configuration interaction and EOM-IP-CCSD results for prototypical charge transfer systems: Noncovalent ionized dimers. *J. Chem. Phys.* **2007**, *127*, No. 164110.
(45) Amos, T.; Woodward, M. Configuration interaction wave-functions for small π systems. *J. Chem. Phys.* **1969**, *50*, 119−123.
(46) Roos, B. O.; Taylor, P. R.; Siegbahn, P. E. M. A complete active space SCF method (CASSCF) using a density matrix formulated super-CI approach. *Chem. Phys.* **1980**, *48*, 157−173.

(47) Casanova, D.; Slipchenko, L. V.; Krylov, A. I.; Head-Gordon, M. Double spin-flip approach within equation-of-motion coupled cluster and configuration interaction formalisms: Theory, implementation and examples. *J. Chem. Phys.* **2009**, *130*, No. 044103.
(48) Casanova, D.; Head-Gordon, M. Restricted active space spin-flip configuration interaction approach: Theory, implementation and examples. *Phys. Chem. Chem. Phys.* **2009**, *11*, 9779−9790.
(49) Bell, F.; Zimmerman, P. M.; Casanova, D.; Goldey, M.; Head-Gordon, M. Restricted active space spin-flip (RAS-SF) with arbitrary number of spin-flips. *Phys. Chem. Chem. Phys.* **2013**, *15*, 358−366.
(50) Ohno, K. Some remarks on the Pariser-Parr-Pople method. *Theor. Chim. Acta* **1964**, *2*, 219−227.
(51) Ramasecha, S.; Soos, Z. G. Optical excitations of even and odd polyenes with molecular PPP correlations. *Synth. Met.* **1984**, *9*, 283−294.
(52) Luzanov, A. V.; Wulfov, A. L.; Krouglov, V. O. A wavefunction operator approach to the full-CI problem. *Chem. Phys. Lett.* **1992**, *197*, 614−619.
(53) Lischka, H.; , et al. *COLUMBUS, an ab initio electronic structure program*, release 7.0; 2012.
(54) Lischka, H.; et al. High-level multireference methods in the quantum-chemistry program system COLUMBUS: Analytic MR-CISD and MR-AQCC gradients and MR-AQCC-LRT for excited states, GUGA spin-orbit CI and parallel CI density. *Phys. Chem. Chem. Phys.* **2001**, *3*, 664−673.
(55) Krylov, A. I.; Gill, P. M. W. Q-Chem: An engine for innovation. *WIREs Comput. Mol. Sci.* **2013**, *3*, 317−326.
(56) Shao, Y.; Fusti-Molnar, L.; Jung, Y.; Kussmann, J.; Ochsenfeld, C.; Brown, S.; Gilbert, A. T. B.; Slipchenko, L. V.; Levchenko, S. V.; O'Neill, D. P.; et al. Advances in Methods and Algorithms in a Modern Quantum Chemistry Program Package. *Phys. Chem. Chem. Phys.* **2006**, *8*, 3172−3191.
(57) Izmaylov, A. F.; Mendive-Tapia, D.; Bearpark, M. J.; Robb, M. A.; Tully, J. C.; Frisch, M. J. Nonequilibrium Fermi golden rule for electronic transitions through conical intersections. *J. Chem. Phys.* **2011**, *135*, No. 234106.
(58) Lee, M. H.; Dunietz, B. D.; Geva, E. Calculation from first principles of intramolecular golden-rule rate constants for photo-induced electron transfer in molecular donor-occeptor systems. *J. Phys. Chem. C* **2013**, *117*, 23391−23401.
(59) Luzanov, A. V. In *Many-body problem in quantum chemistry*; Mestechkin, M. M., Ed.; Naukova Dumka: Kiev, Ukraine, 1987; p 53.
(60) Prezhdo, O. V.; Rossky, P. J. Evaluation of quantum transition rates from quantum-classical molecular dynamics simulations. *J. Chem. Phys.* **1997**, *107*, 5863−5878.
(61) Desouter-Lecomte, M.; Lorquet, J. C. Nonadiabatic interactions in unimolecular decay. IV. Transition probability as a function of the Massey parameter. *J. Chem. Phys.* **1979**, *71*, 4391−4403.
(62) Luzanov, A. V. Spin-free quantum chemistry: What one can gain from Fock's cyclic symmetry. *Int. J. Quantum Chem.* **2011**, *111*, 4042−4066.
(63) Clark, A. E.; Davidson, E. R. Local spin. *J. Chem. Phys.* **2001**, *115*, 7382−7340.
(64) Luzanov, A. V.; Prezhdo, O. V. High-order entropy measures and spin-free quantum entanglement for molecular problems. *Mol. Phys.* **2007**, *105*, 2879−2891.
(65) Head-Gordon, M.; Maslen, P. E.; White, C. A. A tensor formulation of many-electron theory in a nonorthogonal single particle basis. *J. Chem. Phys.* **1998**, *108*, 616−625.